served in any other FOC or WFPC2 images to date, raising the possibility that this feature is related to the approaching comet fragments. An analysis of this emission feature and magnetic field tracing are presented by Prangé *et al.* (*28*).

REFERENCES AND NOTES

1. C. S. Shoemaker, E. M. Shoemaker, D. H. Levy, *Int. Astron. Union Circ. 5725* (1993); J. V. Scotti and H. J. Melosh, *Nature* **365**, 733 (1993); D. K. Yeomans and P. Chodas, *Minor Planet Circ. 22197* (1993).
2. H. B. Hammel *et al.*, Science **267**, 1288 (1995).
3. M. B. Boslaugh, D. A. Crawford, A. C. Robinson, T. G. Trucano, *Geophys. Res. Lett.* **21**, 1555 (1994).
4. F. Herbert, *ibid.*, p. 1047; W. H. Ip and R. Prangé, *ibid.*, p. 1051; P. Kellog, *ibid.*, p. 1055; O. Bolin and N. Brenning, *ibid.*, p. 1063; W. Farrell *et al.*, *ibid.*, p. 1067.
5. J. Sommeria, L. Ben Jaffel, R. Prangé, in preparation.
6. V. Dols *et al.*, *Geophys. Res. Lett.* **19**, 1803 (1992); J. Caldwell *et al.*, *Science* **257**, 1512 (1992); J. C. Gérard, V. Dols, F. Paresce, R. Prangé, *J. Geophys. Res.* **98**, 18793 (1993); J. T. Clarke *et al.*, in preparation.
7. Fragment designations are given by H. A. Weaver *et al.*, *Science* **267**, 1282 (1995).
8. J. T. Trauger *et al.*, *Astrophys. J.* **435**, L3 (1994); J. Holtzman *et al.*, *Publ. Astron. Soc. Pac.*, in press. Images were reduced by (i) subtraction of a flat bias level and scaled dark frames, (ii) division by a flat field image including the detector pixel to pixel response, telescope illumination pattern, and Wood's filter vignetting, and (iii) cosmic ray removal. Finally, the images were corrected for geometric distortion and image shift introduced by the MgF_2 field flattener on the charge-coupled device (CCD) detectors.
9. The edge-finding algorithm consists of (i) finding points of inflection in radial intensity scans over a range of angles on the sunlit limb, (ii) shifting a projected oblate spheroid (an ellipse) of the proper shape, angle, and size of Jupiter in x and y to obtain the statistical best fit to the edge points, and (iii) correcting the east-west location by a measured systematic shift of the observed inflection points from the true limb from a model of the instrument point spread function and limb darkening of Jupiter.
10. As part of the standard data processing, the FOC images were flat fielded and corrected for the geometric distortion resulting from the optical elements and the detector. Locations on Jupiter are determined in the same way as for WFPC2, except that the FOC response provides the polar limb, which can be fit with a model oblate spheroid. A preliminary processing was applied to improve the visibility of features against the noise with a two-dimensional spatial filtering code based on a comparison of counts on Jupiter with the statistics in a background region.
11. A small amount of limb brightening has been added in the lower plots to assist viewing of the absorption regions, rather than correcting for the actual limb darkening.
12. R. A. West *et al.*, *Science* **267**, 1296 (1995).
13. R. Wagener *et al.*, *Icarus* **63**, 222 (1985).
14. W. R. Pryor and C. W. Hord, *ibid.* **91**, 161 (1991).
15. R. Wagener and J. Caldwell, *ibid.* **74**, 141 (1988).
16. W. M. Harris *et al.*, in preparation; R. Prangé *et al.*, *Int. Astron. Union Circ. 6040* (1994); W. Harris *et al.*, *ibid.*; G. Ballester *et al.*, in preparation.
17. K. Noll *et al.*, *Science* **267**, 1307 (1995).
18. At Jupiter's rotation rate of 36°/hour, the rotational smearing in the 400- to 800-s exposures was 4° to 8° in longitude.
19. T. E. Cravens, *Geophys. Res. Lett.* **21**, 1075 (1994).
20. J. T. Clarke, H. W. Moos, S. K. Atreya, A. L. Lane, *Astrophys. J.* **241**, L179 (1980).
21. W. M. Harris *et al.*, in preparation; T. A. Livengood, D. F. Strobel, H. W. Moos, *J. Geophys. Res.* **95**, 10375 (1990).
22. J. E. P. Connerney, in *Planetary Radio Emission*, H. Rucker, M. L. Kaiser, S. J. Bauer, Eds. (Austrian Academy of Science Press, Vienna, 1992), vol. 3, p. 13; personal communication. Magnetic field estimates are for the O_6 model plus current sheet.
23. Brightnesses are estimated for the emissions included in each bandpass using a preliminary estimate for the mean sensitivity at the time of comet impacts (10 days after the most recent WFPC2 decontamination) of 0.0045 electrons s^{-1} per WFC pixel for a 10-kR emission.
24. J. H. Waite *et al.*, *J. Geophys. Res.* **99**, 14799 (1994); J. H. Waite *et al.*, in preparation.
25. I. De Pater *et al.*, in preparation.
26. T. I. Gombosi and A. F. Nagy, *J. Geophys. Res.* **94**, 359 (1989).
27. A. J. Dessler and T. W. Hill, *Bull. Am. Astron. Soc.* **26**, 1593 (1994).
28. R. Prangé *et al.*, *Science* **267**, 1317 (1995).
29. This work is based on observations with the National Aeronautics and Space Administration (NASA)–European Space Agency (ESA) Hubble Space Telescope, obtained at the Space Telescope Science Institute (STScI), which is operated by the AURA for NASA under contract NAS5-26555. We acknowledge R. A. West for access to near-UV images before publication, the data reduction group at the STScI for assistance in the reduction of the images, and our Comet Science Team colleagues M. McGrath and K. Noll for helpful discussions. This research was supported by grant GO-5624.18-93A from the STScI to the University of Michigan. We also acknowledge the INSU–Programme National de Planetologie, CNRS–Action Concertee Sol-Espace support, the Scientific Director of ESA for travel support for R. Prangé, and F. Paresce and D. Grodent for helpful discussions on FOC analysis.

HST Spectroscopic Observations of Jupiter After the Collision of Comet Shoemaker-Levy 9

K. S. Noll, M. A. McGrath, L. M. Trafton, S. K. Atreya, J. J. Caldwell, H. A. Weaver, R. V. Yelle, C. Barnet, S. Edgington

Ultraviolet spectra obtained with the Hubble Space Telescope identified at least 10 molecules and atoms in the perturbed stratosphere near the G impact site, most never before observed in Jupiter. The large mass of sulfur-containing material, more than 10^{14} grams in S_2 alone, indicates that many of the sulfur-containing molecules S_2, CS_2, CS, H_2S, and S^+ may be derived from a sulfur-bearing parent molecule native to Jupiter. If so, the fragment must have penetrated at least as deep as the predicted NH_4SH cloud at a pressure of approximately 1 to 2 bars. Stratospheric NH_3 was also observed, which is consistent with fragment penetration below the cloud tops. Approximately 10^7 grams of neutral and ionized metals were observed in emission, including Mg II, Mg I, Si I, Fe I, and Fe II. Oxygen-containing molecules were conspicuous by their absence; upper limits for SO_2, SO, CO, SiO, and H_2O are derived.

Ultraviolet (UV) spectroscopic observations of Jupiter were made with the Hubble Space Telescope's (HST) Faint Object Spectrograph (FOS) and Goddard High-Resolution Spectrograph (GHRS) both before and after the impacts of the fragments of periodic comet Shoemaker-Levy 9 (SL9). Four different instrument configurations were used to obtain nearly complete spectral coverage from 1250 to 3300 Å (Table 1).

Our spectroscopic program was concentrated on the area near the G impact site (*1*). All observations tracked a spot on Jupiter's surface at the position given in Table 1. Because the observations must be planned in advance, we allowed for small offsets from the best available predicted entry position of the G fragment (*2*). The actual position of the G impact was south and west of the prediction, and we adjusted the offsets accordingly. During an exposure, the position of the aperture drifts slightly in longitude and latitude because of the constant offset. The most extreme movements of the aperture occur when the target is close to a limb and amount to a drift of as much as 15° in longitude during one orbit. However, for most observations the drift is much less. Drifts in latitude are no more than 2°. Errors in pointing from uncertain guide star positions can be as large as 0.7 arc sec (1σ), or about 3° of latitude and 3° of longitude near the central meridian and as much as 10° of longitude near the limb.

One exception to our study of the G impact site occurred on 23 August when the drift of the G site carried it beyond our offset limit. We pointed instead at the predicted position of the L impact complex. The spatial distribution of dark material at the impact sites was very complex

K. S. Noll, M. A. McGrath, and H. A. Weaver are with the Space Telescope Science Institute, 3700 San Martin Drive, Baltimore, MD 21218, USA. L. M. Trafton is with the Department of Astronomy, University of Texas, Austin, TX 78712, USA. S. K. Atreya and S. G. Edgington are with the Atmospheric, Oceanic, and Space Sciences Department, University of Michigan, Ann Arbor, MI 48109, USA. J. J. Caldwell and C. Barnet are with the Institute for Space and Terrestrial Science, Space Astrophysics Laboratory, 4850 Keele Street, North York, Ontario, M3J 3K1, Canada. R. V. Yelle is with the NASA/Ames Research Center, Moffett Field, CA 94035, USA.

within days of the impact (3). Coupled with our pointing uncertainties, this makes it difficult to know precisely what the debris structure in our aperture might be for any given observation. In general, we attempted to point at the darkest available regions (4). The latitudes and longitudes of the center of the aperture for all exposures are listed in Table 1.

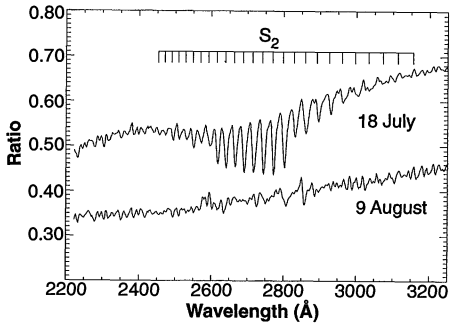

Fig. 1. Spectra obtained with the FOS G270H on 18 July and 9 August ratioed to a preimpact spectrum obtained on 14 July are shown. The spectrum has been smoothed with a 9.3 Å boxcar. At least 16 bands of the S_2 $B\,^3\Sigma_u^- \rightarrow X\,^3\Sigma_g^-$ transition are observable in the 18 July ratio. The bands are also visible in the spectrum obtained on 21 July shown in Fig. 3. By 9 August, there is no trace of S_2 absorption relative to 14 July, though the reflectivity remains approximately half of the preimpact value. A spectrum obtained on 23 August is essentially identical to the 9 August spectrum. The features in the 9 August ratio are mostly due to small wavelength shifts between it and the 14 July spectrum.

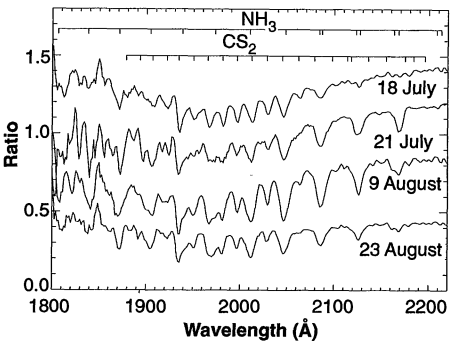

Fig. 2. Spectra obtained with the FOS G190H on 18 July, 21 July, 9 August, and 23 August are shown here divided by a spectrum obtained at the same location on Jupiter on 14 July, before the first impact. The spectrum has been smoothed with a 6.6 Å boxcar, and we have not shown the spectra below 1800 Å, where noise from scattered visible light in the FOS becomes significant. The 18 July, 21 July, and 9 August ratios have been offset by +0.9, +0.7, and +0.3 respectively. A series of strong bands are visible in the ratio spectrum, which we have identified as being due to CS_2 and NH_3. The relative strength of the CS_2 and NH_3 bands can be seen to vary, with the NH_3 becoming more prominent relative to CS_2 in the spectra after 18 July.

Spectral Identifications

The reflection spectrum of Jupiter in the UV is dominated by the spectrum of the sun. From 1600 through 3300 Å, the solar flux increases by a factor of 10^4. In addition, many very strong absorption lines occur in the solar spectrum at almost all wavelengths. To interpret a planetary spectrum, the solar spectral features must be removed. Ordinarily this is done by dividing by a solar spectrum matched to the resolution of the observations as closely as possible. For determination of molecular abundances and aerosol distributions, the reflectance spectrum produced in this way is required. However, for identification of changes in Jupiter's spectrum after the comet impacts, we were able to use the technique of dividing spectra obtained after impact to those obtained before. This method reduces spurious features introduced by Raman scattering in Jupiter's atmosphere and by systematic instrumental effects. Wavelength mismatches are also minimized. Some caution must be exercised because the spectra were not all obtained at the same emission angle, but this effect is not dominant in the ratio spectra we have produced.

Absorption bands. The most striking features in the ratio spectra are the progression of bands in the 2600 to 3000 Å wavelength region (Fig. 1) and a series of strong bands in the 1800 to 2200 Å interval. These features are clearly due to molecular absorption that was present after the impacts of

Table 1. Observation summary. Mean times and emission angles are listed. We list the FOS G190H and G270H exposures separately. Uncertainties in pointing are at least ±3° in latitude and longitude.

Date	Time (UT)	System III latitude, longitude	Emission angle	Instrument	Wavelength range (Å)
13 July	19:57	−48.7, 27.8	61	GHRS	2236 to 2364
14 July	18:22	−48.7, 18.0	66	FOS	2200 to 3300
14 July	18:41	−48.7, 18.0	73	FOS	1650 to 2300
18 July	10:46	−49.2, 18.1	50	FOS	2200 to 3300
18 July	11:06	−49.2, 18.1	54	FOS	1650 to 2300
18 July	19:00	−49.5, 24.5	61	GHRS	2236 to 2364
19 July	06:20	−50.6, 21.3	48	GHRS	2236 to 2324
19 July	15:56	−50.0, 23.3	47	GHRS	1250 to 1535
20 July	11:15	−50.0, 20.8	50	GHRS	1250 to 1535
20 July	12:48	−50.0, 20.8	56	GHRS	1250 to 1535
21 July	16:00	−49.7, 28.8	79	FOS	2200 to 3300
21 July	16:13	−49.7, 28.8	73	FOS	1650 to 2300
21 July	17:44	−50.0, 21.8	47	GHRS	1530 to 1810
22 July	13:07	−49.5, 23.5	49	GHRS	2236 to 2324
22 July	14:40	−49.5, 23.5	57	GHRS	2236 to 2364
09 August	10:28	−49.5, 28.7	74	FOS	2200 to 3300
09 August	10:42	−49.5, 28.7	79	FOS	1650 to 2300
10 August	23:40	−48.6, 31.4	51	GHRS	1530 to 1810
23 August	01:05	−47.2, 10.4	63	FOS	2200 to 3300
23 August	01:18	−47.2, 10.4	67	FOS	1650 to 2300

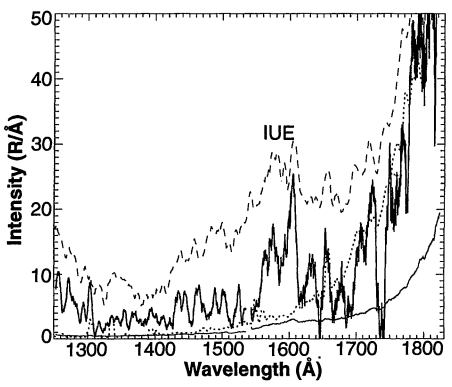

Fig. 3. Jupiter's far-UV spectrum at the impact site of the G fragment. The figure is a mosaic of two settings of grating G140L smoothed to 4.4 Å effective resolution below 1550 Å and smoothed to 7.3 Å resolution at longer wavelengths. The shorter wavelength section is the average of spectra observed on 19 and 20 July 1994, and the longer wavelength section was observed on 21 July. The G impact site spectrum is indicated by the upper solid line, with the propagated error vector shown below. The dotted line is the Solar Ultraviolet Spectral Irradiance Monitor solar spectrum similarly smoothed and scaled to show the location of the continuum if Jupiter were grey. The impact site spectrum shows extensive emission features relative to the diffusely reflected solar continuum. Except above 1770 Å, where the propagated error becomes large, the structure of the emission spectrum appears to be real. The dashed line is a smoothed International Ultraviolet Explorer spectrum of Jupiter's aurora (arbitrary scaling), showing the general correspondence with the impact site spectrum, particularly the H_2 Lyman-band emission near 1600 Å and the H_2 Werner-Lyman emissions near 1250 Å where our spectrum stops. However, the impact site spectrum is much weaker than Jupiter's auroral spectrum and is comparable to the equatorial dayglow (*10*). The bulk of the emission is probably H_2 dayglow. There appear to be strong absorption features between 1650 and 1750 Å that are not identified, although both C_2H_2 and H_2O absorb in this region.

SL9, but was weaker or absent before impact. Identification of the molecules responsible for these absorption bands is based on the match of the positions of the bands to positions measured by laboratory spectroscopy.

The S_2 molecule was not anticipated and has been observed in only one other astronomical source (5). The regularity of the structure near 2800 Å is characteristic of simple molecules, particularly diatomics. The spacing between the bands is between 18 and 42 Å, an energy separation of 297 to 427 cm^{-1}. This small separation between bands suggests a heavy molecule. We were able to match the observed locations unambiguously with the expected positions of the S_2 B-X band system. Figure 1 shows an expanded view of the 18 July and 9 August ratio spectra, along with a stick diagram indicating the laboratory positions of S_2 bands 0-0 (3156 Å) through 25-0 (2454 Å). The increase in band strength shortward of 2820 Å corresponding to bands with upper state vibrational quantum number $v' \geq 10$ is due to the onset of predissociation. The shortened lifetime for these predissociated upper states causes relatively broad lines that are better absorbers than the narrow lines from unpredissociated states.

In the interval from 1800 to 2200 Å, we have identified two molecules responsible for the series of absorption bands: NH_3 (6) and CS_2 (7). The spacing between CS_2 bands is approximately half the spacing between NH_3 bands (Fig. 2). With the exception of features at 1871, 2086, 2125, and 2165 Å, most of the NH_3 bands are blended with bands of CS_2. The sequence of ratio spectra (Fig. 2) shows changes in the relative strengths of the bands, with features that are purely CS_2 weakening relative to features that contain NH_3 bands, which is additional evidence for the presence of both absorbers in the stratosphere.

The shape of the ratio spectra suggests the presence of a continuum absorber in addition to CS_2 and NH_3. Analysis of albedo spectra indicate that the addition of H_2S improves the fit of models to the data. H_2S has a broad absorption with the cross section peaking at ~2000 Å and broad wings falling to half peak at ~1850 and 2130 Å. The identification of H_2S is less certain than the identification of molecules with discrete spectral features.

Below 1800 Å, the albedo determined from the GHRS spectrum (Fig. 3) drops to very low values. This could be due to an increase of C_2H_2 over the preimpact abundance or to the introduction of a modest amount of H_2O in the stratosphere or both.

Emission lines. The 21 July FOS G270H spectrum of the G impact site (Fig. 4) taken near the limb reveals the presence of pronounced metallic emission lines. The most

Table 2. Derived abundances and masses of atoms and molecules observed in emission. This table lists the *g* factor integrated over all transitions within the FOS spectral range for each species. Many of the spectra (Si I, Fe I, Fe II, and CS) are complex, consisting of many lines. For consistency, we used vacuum wavelengths throughout this paper.

Atoms and molecules	*g* factor at 1 AU	Brightness (R)	Column abundance	Mass (g) in aperture	Mass (g) in 10^{15}-g comet
CS	5.8×10^{-4}	5000	2×10^{14}	8.6×10^{8}	3.6×10^{13}
Mg I	5.8×10^{-2}	1450	7×10^{11}	2.3×10^{6}	3.8×10^{13}
Mg II	1.9×10^{-1}	6300	9×10^{11}	2.9×10^{6}	3.8×10^{13}
Si I	8.1×10^{-3}	1100	4×10^{12}	1.5×10^{7}	8.1×10^{13}
Fe I	1.8×10^{-2}	700	1×10^{12}	7.6×10^{6}	4.5×10^{13}
Fe II	5.8×10^{-3}	1000	5×10^{12}	3.8×10^{7}	4.5×10^{13}

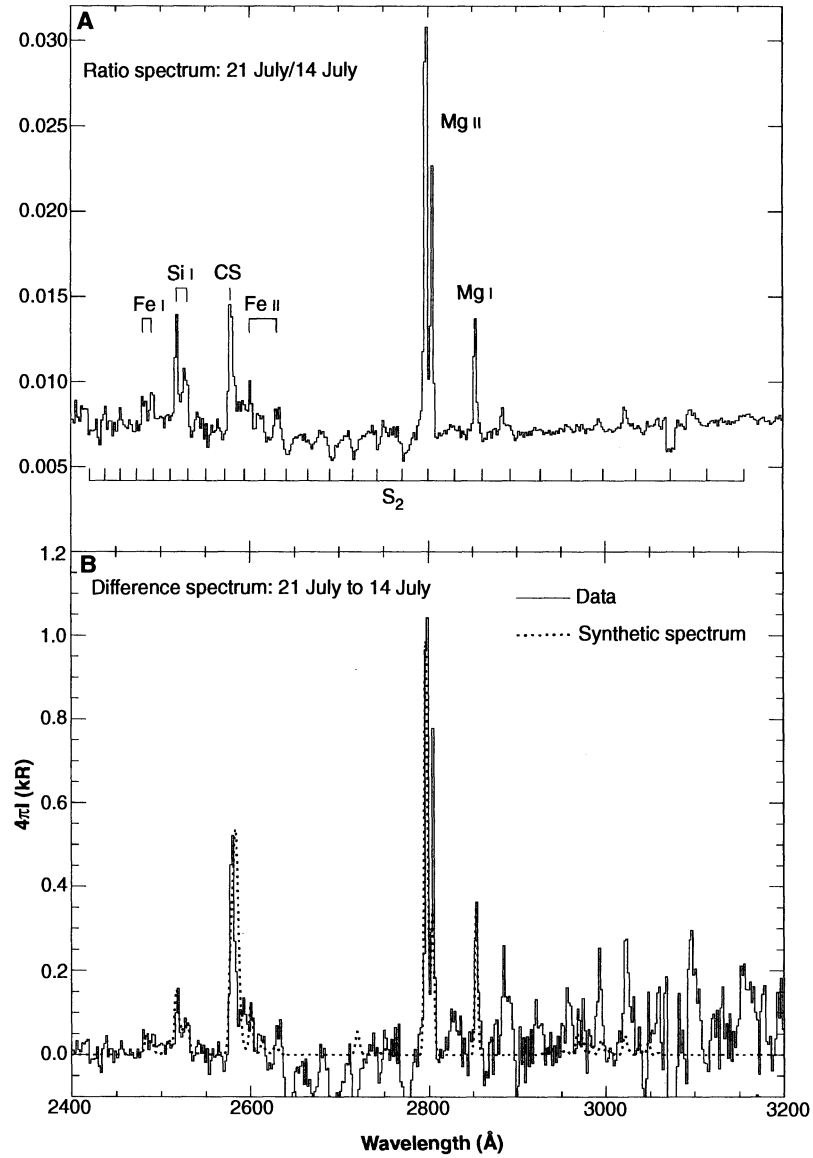

Fig. 4. The FOS G270H spectrum obtained on 21 July is shown divided by the 14 July spectrum in (**A**) and with a scale 14 July spectrum subtracted in (**B**). A model fit of fluorescent emission is also shown with the data in (B). The 21 July spectrum was taken with the FOS aperture close to Jupiter's limb covering both the G impact site and the site of the impact of fragment S 45 min earlier. Because of strong limb darkening and because at the start of the exposure part of the aperture was off the limb, the flux level in the 21 July exposure is significantly lower than in the 14 July spectrum. As on 18 July, a number of S_2 absorption bands were observed in this spectrum. In addition, several strong emission lines are seen in the spectrum. Lines from Mg, Mg^+, Si, Fe, and CS are definitely identified. Other emission lines are unidentified.

likely excitation mechanism for these features is solar fluorescence (8). We show the emission spectrum in the form of both a ratio and a difference with the preimpact baseline observation on 14 July. Absolute intensities (that is, the difference spectrum) of the emission features are required in order to estimate column abundances; however, the signal-to-noise ratio deteriorates toward the long-wavelength end of this spectrum because of the difficulty in matching the continuum levels of the two spectra. Cross-comparison of the features apparent in both the ratio and difference spectra provides the most reliable indication of what is real.

Identifications of neutral and singly ionized magnesium (Mg I, 2853 Å and Mg II, 2796 to 2805 Å) are obvious because of their location at the minima of the strongest solar Fraunhofer absorption lines from these elements in the Jupiter reflection spectrum. Identifications of emissions from neutral and singly ionized iron (Fe I and Fe II), neutral silicon (Si I), and molecular emission from the 0-0 transitions of carbon monosulfide (CS) are based on comparison of calculated relative fluorescent intensities for likely candidate species with the observed emission spectrum (Fig. 4) (9).

The solar excitation rate and radiative decay rate of each relevant transition were calculated for all the detected species. The results of these calculations are summarized in Table 2. Column abundance was calculated from a full spectral calculation for each molecule and a fit of the synthetic spectra to the observed spectrum. For all the transitions except Mg I, the *g* factors (fluorescence efficiency factor) values are formally temperature dependent, but the temperature dependence does not appear to be strong for the cases tested. We used a temperature of 1000 K for all cases. Many of the observed transitions are mildly optically thick. In these cases, the derived abundances should be viewed as lower limits; however, because the optical depths are in no case extremely large, the estimates given here should be reasonably accurate.

Several emission features remain unidentified, including particularly the features near 2884 and 3096 Å. For the 2884 Å feature, we considered Si I at 2881 Å, but the wavelength mismatch is larger than for any of the other positively identified features, a detectable Si I line at 2881 Å is inconsistent with our fluorescence calculations, and this emission line does not sit at the bottom of the strong solar Si I 2881 Å Fraunhofer line. For the 3096 Å feature, we considered OH 3090 Å and Al I 3092 Å. Again, however, the wavelength mismatch is larger than that for other positively identified features. Weak emission lines may also be present in the spectra obtained on other dates, in particular, weak emission features appear near the position of the CS 0-0 transitions on spectra from 18 July through 23 August.

There is little doubt that the metals come from the SL9 impacts, because the elements observed are not present in Jupiter's upper atmosphere. The presence of metals high in the jovian atmosphere could be due to both material ablated from the impactors during the entry (bolide) phase and impactor debris lifted high into the atmosphere by the plumes and ultimately deposited into the stratosphere.

The 1250 to 1840 Å spectrum of the G impact site (Fig. 3) includes contributions from the diffusely reflected solar spectrum, the superposed Io torus, and Jupiter's dayglow. Below 1610 Å, the spectrum is dominated by emission. At the time of the 1250 to 1550 Å observations, the Io torus was tilted largely out of the field of view of the GHRS and its contribution is expected to be small. The dominant component of the emission appears to be the H_2 dayglow spectrum (*10*). Integrating the observed spectrum for the G fragment site over the observed wavelength interval leads to an emission intensity of approximately 2.6 kilorayleighs (kR) for all sources, which is in reasonable agreement with other measurements of the jovian H_2 dayglow. In this context, we identify the broad S^+ feature at 1258 Å as a possible consequence of the G fragment impact. This feature consists of S^+ lines at 1259.3, 1253.8, and 1250.5 Å in a 3:2:1 ratio. The integrated intensity of the three S^+ lines is 93 R, comparable to the 117 ± 18 R total intensity of S^+ observed in Io's torus on 24 July (*11*). However, as we have argued above, the Io torus appears to be a minor contributor to the observedspectrum, which suggests that the S^+ we observed is jovian in origin.

Table 3. Derived vertical column abundances and masses of molecules observed in absorption. Masses in Jupiter are computed with the use of the area of the FOS aperture, most likely an underestimate of the total area of perturbed atmosphere. The mass of each element derived from the observed column is also listed with the element identified in parentheses. The mass of each element that could be contributed by the impactor is based on a total mass of 10^{15} g, corresponding to a comet of diameter 1.24 km and bulk density 1 g cm^{-3}. This is near the median of sizes estimated by a variety of means (*27*).

Molecule	Column abundance (cm^{-2})	Mass (g) (element) in aperture	Mass (g) (element) in 10^{15}-g comet
NH_3	$0.5–2 \times 10^{16}$	$1–4 \times 10^{10}$(N)	2×10^{13}(N)
S_2	$1–10 \times 10^{18}$	$0.9–9 \times 10^{13}$(S)	4×10^{13}(S)
CS_2	$0.5–2 \times 10^{15}$	$0.4–2 \times 10^{10}$(S)	
H_2S	$2–5 \times 10^{16}$	$0.9–2 \times 10^{11}$(S)	
SO_2	$\leq 9 \times 10^{15}$	$\leq 4 \times 10^{10}$(O) $\leq 4 \times 10^{10}$(S)	5×10^{14}(O)
SO	$\leq 4 \times 10^{15}$	$\leq 1 \times 10^{10}$(O) $\leq 2 \times 10^{10}$(S)	
CO	$\leq 6 \times 10^{14}$	$\leq 1 \times 10^{9}$ (O)	
SiO	$\leq 1 \times 10^{16}$	$\leq 5 \times 10^{10}$(Si) $\leq 3 \times 10^{10}$(O)	2×10^{14}(Si)
H_2O	$\leq 5 \times 10^{18}$	$\leq 1 \times 10^{13}$(O)	

Determination of Abundances of Selected Molecules and Atoms

We discuss in some detail the derivation of abundance estimates for two gases, S_2 and NH_3, because of their significance. We also derive upper limits to O-containing molecules, which are conspicuous by their absence. Preliminary abundance determinations for other molecules are given in Table 3 (*12*). In the cases of CS_2, SO, and SO_2, the cross sections we used are valid only for low column abundances of these gases. Either additional laboratory work or line-by-line modelling of these molecules will be required to investigate the possible effects of line saturation that would lead us to underestimate the total abundances of these gases. The effects of aerosols have been incompletely constrained, so reported abundances cannot be reliably converted to mole fractions.

Sulfur. To obtain a preliminary estimate of the abundance of S_2, we calculated a line-by-line transmission spectra using a line listing generated from published S_2 molecular parameters (*13*). We modeled the atmosphere as isothermal and homogeneous, with a nominal value of 300 K. It is worth noting, however, that much higher rotational temperatures would reduce the derived S_2 abundance. Five bands were used to derive abundance estimates, the 5-0 through 9-0 bands; bands at shorter wavelengths were not used because the predissociation line widths are not accurately known. On the basis of the match between the equivalent widths of the calculated and observed spectra, we estimated the absorbing column at $N = 10^{19}$ cm^{-2} with a factor of 3 uncertainty. A simple reflecting layer model then implies a vertical column of 3×10^{18} cm^{-2}. Unlike other molecules detected by us, S_2 cross sections have not been directly measured in the laboratory. A more thorough analysis using all

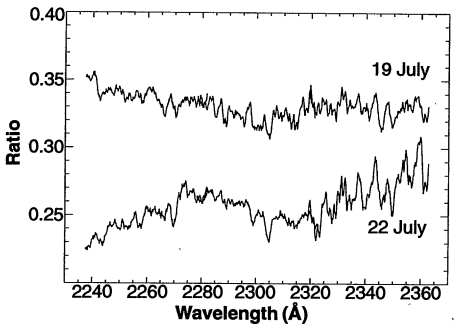

Fig. 5. Three different grating settings were used to record GHRS spectra from 2236 to 2364 Å on 13 July, 18 to 19 July, and 22 July. The spectra from 18 to 19 July and 22 July were ratioed to the 13 July spectrum. Small normalization factors have been applied to the individual segments based on the intervals where spectra overlap. The 22 July spectrum was then offset by −0.08 for clarity. The slope of the ratio spectrum shortward of 2280 Å is significantly greater than in the 19 July ratio. H_2S is one potential absorber that could affect this slope. Some of the apparent features in the ratio spectra are the result of slight wavelength mismatches between the data from 13 July and later. However, several features appear to be real, in particular the absorption feature centered at 2305 Å, which is also detectable in FOS scans through 23 August. The depth of this feature is 8%. The absence of a detectable feature with a depth of 17% or more at the positions of the 0-0, 1-0, and 2-0 bands of SiO leads to an upper limit of $N \leq 10^{16}$ cm^{-2}.

the bands and measured cross sections is clearly needed, and conclusions based on the abundance of S_2 determined here should be weighted accordingly.

If S_2 is uniformly distributed within the FOS field of view, a total mass of S_2 molecules of 2.5×10^{13} g is implied. The derived column abundance implies that individual lines in the S_2 bands are strongly saturated at 300 K. Therefore, the mass estimate is a lower limit to the mass, because any other assumption about the horizontal distribution of S_2 in our aperture will require larger values for the total mass to fit the observed band depths. Of course, it is also likely that the areal extent of the S_2 is significantly greater than the projected area of the FOS aperture, leading to even higher mass estimates. We discuss this in more detail below.

S_2 was present in the spectrum obtained on 21 July (Fig. 4) but was absent when we next observed on 9 August. In the same spectrum, copious NH_3 and CS_2 were observed, implying that the lifetime of S_2 in Jupiter's stratosphere is $t_{S_2} < 19$ days. Indeed, a simple calculation yields a lifetime against photodissociation for the entire column of S_2 that is on the order of hours. A more detailed calculation (*14*) finds that the S_2 column decreases by a factor of 6 in the first hour but more slowly thereafter because of efficient recycling of S_2 over a limited pressure range. Therefore, it is possible that our observation 3 hours after the G impact sampled only a fraction of the initial column of S_2.

Ammonia. We carried out a series of radiative transfer-scattering calculations and compared them to the 18 July reflectance spectrum. Several vertical profiles of NH_3 were considered, including a photochemical profile (*15*) and a model with NH_3 distributed uniformly in the upper troposphere and the stratosphere. The best fit for NH_3 on 18 July was obtained with a uniform distribution and a vertical column abundance of 1×10^{16} cm^{-2} with a factor of 2 uncertainty. For an effective scattering layer at 100 mbar, this corresponds to a mole fraction of $q_{NH_3} = 1$ part per billion (ppb). This should be compared to the 100-ppb saturation value of NH_3 at Jupiter's 110-K 100-mbar level. Ammonia is not normally present in Jupiter's stratosphere in detectable quantities (except, perhaps, in the equatorial zone), and its presence there after the impacts is one of the major observable effects both in the UV and in the infrared (IR). Retrieval of the NH_3 abundance from UV spectra is independent of small temperature changes, an advantage because perturbations to the temperature profile almost certainly followed the impacts.

CS_2 is required above the effective scattering layer (~100 mbar in the unperturbed jovian atmosphere), with a vertical column abundance of 0.5×10^{15} to 2×10^{15} cm^{-2}. Holding CS_2 constant with altitude was adequate for a good fit. The CS_2 cross sections near 2000 Å were determined with laboratory measurements that had a minimum column abundance of $N_{lab} = 6.3 \times 10^{14}$ cm^{-2}. The maximum line-of-sight column abundance, 6×10^{15} cm^{-2}, is about a factor of 10 greater. It is not clear whether the laboratory cross sections are still on the linear portion of the curve of growth at this point, so CS_2 may be underestimated. Model fits are improved in the 2200 to 2500 Å range by the addition of 2×10^{16} to 5×10^{16} cm^{-2} of H_2S.

Oxygen-containing molecules. Oxygen is normally a rare element in Jupiter's stratosphere, with CO the dominant reservoir at a mole fraction of no more than 100 ppb and probably closer to the tropospheric mole fraction of 1.6 ppb (*16*). We recognized that even an object as small as 10^{15} g would significantly increase the concentration of O-containing molecules over an area thousands of kilometers in diameter. It was also thought that deep-penetrating impactors might excavate significant quantities of jovian oxygen, present as H_2O at pressures greater than 5 to 10 bars. Thermochemistry in the shock and plume can create a large variety of O-bearing species.

Both SO and SO_2 molecules have a series of strong bands in the UV, with the most prominent occurring between 1900 and 2100 Å, that are not consistently aligned with the prominent absorption bands in our ratio spectrum. Several of the strongest SO_2 bands coincide with very weak features in the ratio spectrum, but others do not. We can confidently rule out any absorption with $\tau > 0.1$. The average cross section for the strong bands averaged over 3 Å is 1×10^{-17} cm^2 molecule^{-1} (*17*). Therefore, our upper limit line-of-sight column (3σ) is $N \leq 3 \times 10^{16}$ molecules cm^{-2}. These cross sections are valid for column abundances at least as large as the minimum column used in laboratory measurements, $N_{lab} = 1.3 \times 10^{16}$ cm^{-2}. Similarly, SO has a few bands that are aligned with strong features we have attributed to CS_2, but most are aligned only with weak features or with no features at all. Any SO absorption must have an optical depth of less than 0.1. Because the cross sections for SO are approximately two times stronger than for SO_2, the corresponding upper limit for the SO line-of-sight column is half that of SO_2, $N \leq 1.5 \times 10^{16}$ molecules cm^{-2}.

SiO is a byproduct of silicate ablation in hydrogen atmospheres (*18*) and therefore is a potential tracer of both O- and Si-containing molecules. The strong $A^1\Pi \rightarrow X^1\Sigma$ bands were covered by the GHRS G270M observations (Fig. 5). In our spectral range, there are the 0-0, 1-0, and 2-0 bands centered at 2344.4, 2298.9, and 2255.9 Å, respectively. The spectrum of SiO was synthesized from molecular constants with calculations that fully resolve the line structure of the $A^1\Pi \rightarrow X^1\Sigma$ band. The total absorption is virtually independent of temperature over a range from $T = 150$ to 300 K. An 8% absorption feature at 2305 Å is easily detected in our ratio spectra. On the basis of this, we adopt a conservative upper limit for SiO of $N \leq 10^{16}$ cm^{-2}.

We find an upper limit on the vertical column abundance of stratospheric CO over the G fragment impact site of 6×10^{14} cm^{-2}, based on the lack of detection of emissions at the wavelengths of the 1-0, 2-0, 3-0, and 4-0 4th positive bands at 1510, 1478, 1447, and 1419 Å, respectively. With the assumption that the observations probe to the 100 μbar level, this corresponds to an upper limit on the atmospheric CO mole fraction of 60 ppb (*19*). Far-UV observations probe CO to shallower depths than IR or millimeter-wave observations do and may provide constraints on the vertical distribution of this gas.

Our spectra below 1800 Å can accommodate a vertical column abundance of H_2O as large as $N = 5 \times 10^{18}$ cm^{-2}. However, this is uncertain because H_2O has a broad continuum absorption in this part of the spectrum. Alternatively, the spectrum can be matched with the addition N

$= 10^{19}$ cm^{-2} of C_2H_2 and no H_2O. This amount of C_2H_2 is 10 times greater than that normally found in Jupiter's stratosphere (*20*). The maximum abundance of H_2O corresponds to a mass of 10^{13} g, which is comparable to the mass of S_2 observed.

Discussion

The atomic and molecular masses derived from HST UV spectra are clearly lower limits because of the limited sampling both vertically and horizontally. UV spectra sample the uppermost portion of the stratosphere at the long-wavelength limit of our observations and sample exclusively the stratosphere at wavelengths below ~2000 Å. Large amounts of unusual material could easily have been deposited at pressures below the deepest levels we can probe, and the depth of penetration may be less than in the normal atmosphere because of impact-generated aerosols. In addition, the mass estimates in Table 3 are limited to the mass observed in our relatively small apertures. A UV image obtained on 21 July (*3*) shows dark material in the G-D impact site spread over an area at least 4.3 arc sec east to west and 2.7 arc sec north to south. If we assume that the gas shares the same distribution as the UV dark material and is uniform over this region, then we underestimate the mass of each molecule by at least a factor of 30.

The most striking result in this compilation is the large abundance of S-containing molecules, particularly S_2 and CS. The mass of S_2 in our small aperture alone approaches the total mass of S we would expect from a 10^{15}-g cometary impactor. We might expect slightly more S from an asteroid impactor, but the enhancement is by no more than a factor of 2 (*21*). Similarly, the abundance of S in emission as CS is significantly greater than the column abundances of the metal atoms we observed, despite the fact that in a comet the S/Mg, S/Si, and S/Fe abundance ratios are 0.95, 0.44, and 0.80, respectively (*22*).

It might be possible to derive the observed quantity of S from an impactor if S molecules remain more localized after the impact than either dust or NH_3 gas (*23*) or if we allow for a more massive fragment. However, a fundamental problem with any scenario that derives S from the comet is the large relative abundance of O in comets: S/O = 0.04 (*21*). The low limits on O-containing molecules, particularly SO and SO_2, indicate that the S/O ratio was considerably larger. This argument is not significantly altered if the maximum quantity of H_2O that our observations allow is present.

A reservoir of material where the S/O > 1 exists in a narrow range of altitudes on Jupiter. The undisturbed jovian atmosphere is essentially devoid of H_2S molecules at a pressure (*P*) of 0.5 bar (*24*) and above the NH_4SH cloud tops at P = 1.2 bar (*20*). Below the NH_4SH cloud, H_2S is expected to be the dominant form of S and should be present at a mole fraction equal to the abundance of S in Jupiter, which is likely to be close to the cosmic abundance of sulfur of 3.7×10^{-5}. Below the 2.5-bar pressure level, the saturated vapor pressure mole fraction of H_2O exceeds the cosmic abundance of S, though H_2O is probably subsaturated above the cloud tops of still poorly determined depth between 5 and 10 bars. This narrow altitude range should constrain impact models and impactor sizes. Zahnle and Mac-Low (*25*), for example, predicted that a 0.45-km object of unit density would penetrate to the 2-bar level. A much smaller object would not penetrate deep enough into the atmosphere to reach layers where S is relatively abundant. An object considerably larger would penetrate below the water cloud layer where S/O = 0.027.

Heating of the NH_4SH cloud can lead quite naturally to some of the gases we observe. NH_3 and H_2S are the immediate products of heating. H_2S can be processed further through reactions with energetic hydrogen such as (*26*, *20*):

$$H_2S + H \rightarrow HS + H_2$$

$$HS + HS \rightarrow H_2S + S$$

$$HS + HS \rightarrow H_2 + S_2$$

$$HS + S \rightarrow H + S_2$$

Because the expected mole fraction of H_2S in Jupiter's atmosphere is the solar abundance, 3.7×10^{-5} or more, we can estimate the volume of jovian gas that must have been heated to account for the S molecules observed. If we estimate the total mass of S at 10^{14} g, then a cylinder of jovian atmosphere 10 km thick at 1.6 bar (the approximate thickness of the NH_4SH cloud) and 300 km in diameter is needed to supply to observed material. This may be plausible given the dramatic effects observed with the impacts, but we are left with the problem of why the S/N ratio in the observed debris apparently exceeds 100, whereas in any location on Jupiter the most likely value for the S/N ratio is ≤ 0.16. Conceivably, N in the blast region is converted to molecules such as N_2 and HCN, which are not well constrained by our observations.

If the S we observed is indeed derived from a parent molecule native to Jupiter, it is the first observation of this element in the atmosphere, and bolsters thermochemical equilibrium models that have long predicted the presence of a massive cloud of NH_4SH below a cloud of NH_3 ice. Sulfur chemistry has long been invoked as a mechanism for the coloration of Jupiter's clouds. Because S is sequestered in Jupiter's troposphere, we can constrain the impactor's penetration depth to a minimum of 1 to 2 bars. Alternatively, if the S we observed is derived from the impactor, the mass of the impactor would have to be significantly more than 10^{15} g, the S from the impactor would have to be efficiently transported to the stratosphere where we could observe it in the UV, and somehow reactions between S and O in the plume would have to be damped. A final resolution of this issue may have to await the arrival of the Galileo probe.

Note added in proof: Further modeling of the S_2 absorption bands, making use of recently determined transition moments, Franck-Condon factors, and lifetimes (*28*) that permit analysis of the entire band system, indicate that the S_2 temperatures may be much higher than assumed here (above 1000 K) and the densities much lower. Analysis is not complete, but a lower limit of 10^{16} cm^{-2} appears likely.

REFERENCES AND NOTES

1. We used the 0.86-arc sec diameter circular aperture with the FOS and the 1.74-arc sec square aperture with the GHRS. We used the Red digicon of the FOS. We analyzed FOS G190H data only longward of 1800 Å because of scattered visible-wavelength photons within the FOS. The effective spectral resolution of our observations is 3.3 Å full width at half maximum (FWHM) for the FOS with the G190H grating, 4.6 Å for the FOS G270H, 0.75 Å for the GHRS G270M, and 4.6 Å for the GHRS G140L. These values assume that the aperture was filled with an extended source of uniform brightness. Deviations from this ideal case almost certainly occurred, the most drastic being the 21 July observations with the FOS that began with a portion of the aperture off the limb. In such cases, the values quoted above are upper limits to the FWHM.
2. D. K. Yeomans *et al.*, personal communication. The ephemerides were widely distributed via e-mail and were posted on the World Wide Web.
3. H. B. Hammel *et al.*, *Science* **267**, 1288 (1995); R. A. West *et al.*, *ibid.*, p. 1296; J. Clarke *et al.*, *ibid.*, p. 1302.
4. R. Beebe and A. Simon, personal communication.
5. M. F. A'Hearn, P. D. Feldman, D. G. Schleicher, *Astrophys. J.* **274**, L99 (1983).
6. F. Z. Chen, D. L. Judge, C. Y. R. Wu, J. J. Caldwell, in preparation.
7. H. Xu and J. A. Joens, *Geophys. Res. Lett.* **20**, 1035 (1993); C. Y. R. Wu and D. L. Judge, *ibid.* **8**, 769 (1981).
8. The population of the upper states at thermal equilibrium is comparable for fluorescence processes and thermal excitation with temperatures as low as ~1000 K. However, at densities typical of the upper atmosphere, thermal equilibrium is not achieved, and the collisional excitation rate is orders of magnitude smaller than the fluorescent excitation.
9. All calculations used the solar spectrum from M. F. A'Hearn, J. T. Ohlmacher, D. G. Schleicher, *Technical Report TR AP83-044* (University of Maryland, College Park, MD, 1983) Doppler shifted by 8.6 km s^{-1} to account for the rotation of Jupiter. The molecular data for the CS molecule were provided in the form of a computer program by T. Bergeman of the State University of New York, Stony Brook. Atomic data for Fe I were provided by K. Carpenter of GSFC. Oscillator strengths, lifetimes, energy levels, and branching ratios for all other species were obtained from W. L. Wiese, M. W. Smith, B. M. Miles, *Atomic Transition Probabilities—Sodium Through Calcium*, vol. II, NSRDS-NBS 22, 1969.
10. P. D. Feldman *et al.*, *Astrophys. J.* **406**, 279 (1993), figure 1b. Several broad features can be recognized from the HUT spectrum of Jupiter's equatorial re-

gion. Feldman *et al.* found an H_2 band intensity of 1.6 kR averaged along their slit for wavelengths longer than 1223 Å, a bandpass close to that used in our observations. L. M. Trafton, J. C. Gerard, G. Munhoven, and J. H. Waite, [*Astrophys. J.* **421**, 816 (1994)] had previously detected the jovian equatorial dayglow spectrum with the GHRS and derived a total H_2 emission intensity of about 3.2 kR.
11. M. A. McGrath *et al.*, *Science* **267**, 1313 (1995).
12. Abundances are reported as either line-of-sight column abundance, which takes into account the local emission angle and two-way path through the atmosphere, or vertical column abundance, a one-way column following the local normal vector.
13. Vibrational and rotational constants were obtained from R. F. Barrow and R. P. Du Parcq [*Elemental Sulfur*, B. Meyer, Ed. (Interscience, New York, 1965)]. Lifetimes and transition strengths are from K. A. Meyer and D. R. Crosley, *J. Chem. Phys.* **59**, 1933 (1973); W. H. Smith, *J. Quant. Spectrosc. Radiat. Transfer* **9**, 1191 (1969); and C. R. Quick and R. E. Weston, *J. Chem. Phys.* **74**, 4951 (1981). Franck-Condon factors were obtained from W. R. Anderson, D. R. Crosley, J. E. Allen Jr., *ibid.* **71**, 821 (1979).
14. J. I. Moses, M. Allen, G. R. Gladstone, in preparation.
15. S. K. Atreya, T. M. Donahue, W. R. Kuhn, *Icarus* **31**, 348 (1977); S. K. Atreya and P. N. Romani, in *Planetary Meteorology*, G. E. Hunt, Ed. (Cambridge Univ. Press, 1985), pp. 17–68.
16. K. S. Noll, R. F. Knacke, T. R. Geballe, A. T. Tokunaga, *Astrophys. J.* **324**, 1210 (1988).
17. R. D. Martinez and J. A. Joens, *Geophys. Res. Lett.* **19**, 277 (1992).
18. M. J. Prather, J. A. Logan, M. B. McElroy, *Astrophys. J.* **223**, 1072 (1978).
19. G. P. Tozzi, P. D. Feldman, M. Festou, in preparation. We used a g factor of 1.7×10^7 photons s^{-1} molecule^{-1} at 1 AU for the CO (1-0) band for the quiet sun. The upper limit corresponds to the propagated error at the wavelength of the (1-0) band, which limits the detectability of features in Jupiter's dayglow spectrum, the local continuum for the CO emission bands. The effective width of the (1-0) band was taken to be the effective bandwidth, 2.1 Å. Extinction at the impact site may reduce the visibility of CO, leading to an underestimate of the atmospheric CO mole fraction. E. Lellouch *et al.* [*Bull. Am. Astron. Soc.*, special session on comet Shoemaker-Levy 9, abstract 02.03] derive a CO mole fraction of ~40 ppm for $P \leq$ 300 μbar, considerably higher than our upper limit.
20. S. K. Atreya, *Atmospheres and Ionospheres of the Outer Planets and their Satellites* (Springer-Verlag, New York, 1987), chap. 3 and 5.
21. E. K. Jessburger, J. Kissel, J. Rahe, *The Composition of Comets in Origin and Evolution of Planetary and Satellite Atmospheres*, S. K. Atreya, J. B. Pollack, M. S. Matthews, Eds. (Univ. of Arizona Press, Tucson, AZ, 1989). The S/O ratio used is the number ratio of S/O in comet Halley, assuming a gas/dust ratio of 0.9. S is considerably more abundant in the dust fraction than in the gas, and a gas/dust ratio of 0.9 is near the lower limit of the range determined for this ratio. Comets with less dust would have a correspondingly lower S/O ratio.
22. E. Anders and N. Grevesse, *Geochim. Cosmochim. Acta.* **53**, 197 (1989).
23. G. Orton *et al.*, *Science* **267**, 1277 (1995).
24. H. P. Larson, D. S. Davis, R. Hofmann, G. L. Bjoraker, *Icarus* **60**, 621 (1984).
25. K. Zahnle and M. Mac-Low, *ibid.* **108**, 1 (1994).
26. J. S. Lewis and R. G. Prinn, *Science* **169**, 472 (1970).
27. H. A. Weaver *et al.*, *Science* **263**, 787 (1994). An observational constraint on the size of the impactors comes from the upper limit diameter established by Weaver *et al.* of ~4 km. Several theoretical arguments have led to estimates of diameter of ~1 km for the parent object.
28. S. Langhoff, personal communication.
29. The SL9-Jupiter campaign was the result of the efforts of hundreds of people at the Space Telescope Science Institute and Goddard Space Flight Center. We extend our appreciation to all. P. Feldman helped in the identification of CS_2, provided access to his spectroscopic library, and contributed many thoughtful ideas. D. Gilmore and E. Smith provided assistance at the cost of many hours of missed sleep. H. Hammel was a gracious negotiator in the competition for prime orbits during impact week and provided the images we needed for our initial target acquisition. R. Beebe and A. Simon helped us find the drifting impact sites in the weeks after the impacts. Everyone on the HST science observing team participated during impact week in an open and continuous exchange of ideas for which we are grateful. We also thank D. Leckrone for his enthusiastic support during the most harrowing parts of the impact week. M. A'Hearn and an anonymous referee provided valuable comments on the manuscript. Support provided by NASA through grant GO-5642.14-93 from the STSI, which is operated by the Association of Universities for Research in Astronomy under NASA contract NAS5-26555.

17 November 1994; accepted 7 February 1995

Response of the Io Plasma Torus to Comet Shoemaker-Levy 9

M. A. McGrath, D. T. Hall, P. L. Matheson, H. A. Weaver, J. T. Trauger, T. E. Smith, N. Thomas, R. Gladstone, N. M. Schneider, W. M. Harris, T. A. Livengood, R. Prangé, M. C. Festou

Spectroscopic and imaging observations of the Io plasma torus were made in June and July 1994 in conjunction with the encounter of periodic comet Shoemaker-Levy 9 with Jupiter. Characteristic emissions from sulfur and oxygen ions showed a decline of about 30 percent in the extreme ultraviolet and an increase of about 40 percent in the far ultraviolet relative to preimpact observations. Changes in the extreme ultraviolet may be indicative of small changes in the torus electron temperature as a result of quenching of electrons by dust associated with the comet passage. However, no new emission features indicative of fragment dust within the torus were detected. The characteristic torus morphology seen in ground-based imaging was typical of that observed in the past.

An extensive program of observations was undertaken in July 1994 to determine what effect, if any, comet Shoemaker-Levy 9 (SL9) might have on the Io plasma torus. The torus is composed primarily of sulfur and oxygen species that are ejected as neutral atoms or molecules from the surface and atmosphere of Io, ionized by the plasma, captured by the jovian magnetic field, and swept into a toroidal region surrounding Jupiter near the orbit of Io (*1*). The ejection mechanism is widely thought to be sputtering by energetic charged particles in the torus. The potential for significant change to the torus was believed to exist because dust deposited by the comet into the jovian magnetosphere might be transported to and perturb the torus (*2*).

M. A. McGrath, H. A. Weaver, and T. E. Smith are at the Space Telescope Science Institute, Baltimore, MD 21218, USA. D. T. Hall is in the Department of Physics and Astronomy, Johns Hopkins University, Baltimore, MD 21218, USA. P. L. Matheson is in the Department of Aerospace Engineering, University of Southern California, Los Angeles, CA 90089–1191, USA. J. T. Trauger is at the Jet Propulsion Laboratory, Pasadena, CA 91109, USA. N. Thomas is at the Max-Planck-Institut für Aeronomie, Postfach 20, D-W-3411 Katlenburg-Lindau, Germany. R. Gladstone is at Southwest Research Institute, San Antonio, TX 78238, USA. N. M. Schneider is at the Laboratory for Astronomy and Space Physics, University of Colorado, CB 392, Boulder, CO 80309–0392, USA. W. M. Harris is at the Space Physics Research Laboratory, University of Michigan, Ann Arbor, MI 48109, USA. T. A. Livengood is at the Goddard Space Flight Center, Code 693.1, Greenbelt, MD 20771, USA. R. Prangé is at the Institut d'Astrophysique Spatiale, Orsay, France. M. C. Festou is at the National Center for Scientific Research, Observatoire Midi-Pyrenees, F-31400 Toulouse, France.

Source and Effect of Dust

The comet had extensive dust tails and dust "wings" at both the leading and trailing edges of the train of nuclei (*3*), and more dust came from the continuing fragmentation of the nuclei (*4*). The total mass of dust associated with SL9 was relatively large (*5*). Most of this dust did not impact Jupiter's atmosphere and could thus remain in the jovian magnetosphere for long periods of time, possibly even forming another tenuous jovian ring (*2*). The Ulysses spacecraft detected two dust streams in 1992 compatible with SL9 origin (*6*). We therefore monitored the Io plasma torus carefully near the time of impact (when the comet passed through the inner magnetosphere for a second time) to search for temporal variability and new emissions that might be associated with the SL9 passage.

Effects caused by an enhanced amount of dust in the magnetosphere and torus might include the absorption of torus plasma by the dust; the addition to refractories and ice mantle elements such as H, C, O, N, Si, Mg, or Fe to the torus as a result of ion sputtering of the dust; enhanced sputtering of surface material to the atmosphere and torus from